NANO LETTERS

pubs.acs.org/NanoLett
Letter

Exploiting Topological Darkness in Photonic Crystal Slabs for Spatiotemporal Vortex Generation

Wenzhe Liu,*,⊥ Jiajun Wang,⊥ Yang Tang,⊥ Xinhao Wang, Xingqi Zhao, Lei Shi,* Jian Zi,* and C. T. Chan*

Cite This: https://doi.org/10.1021/acs.nanolett.3c04348

ABSTRACT: Spatiotemporal optical vortices (STOVs) with swirling phase singularities in space and time hold great promise for a wide range of applications across diverse fields. However, current approaches to generate STOVs lack integrability and rely on bulky free-space optical components. Here, we demonstrate routine STOV generation by harnessing the topological darkness phenomenon of a photonic crystal slab. Complete polarization conversion enforced by symmetry enables topological darkness to arise from photonic bands of guided resonances, imprinting vortex singularities onto an ultrashort reflected pulse. Utilizing time-resolved spatial mapping, we provide the first observation of STOV generation using a photonic crystal slab, revealing the imprinted STOV structure manifested as a curved vortex line in the pulse profile in space and time. Our work establishes photonic crystal slabs as a versatile and accessible platform for engineering STOVs and harnessing the topological darkness in nanophotonics.

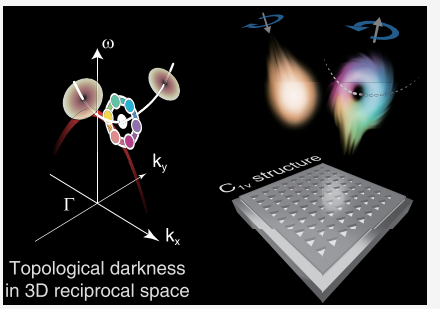

KEYWORDS: *spatiotemporal optical vortex, topological darkness, photonic crystal slab, polarization conversion*

Spatiotemporal optical vortices (STOVs) are light wave packets containing phase singularities that swirl around axes perpendicular to their direction of propagation and carry transverse orbital angular momentum in the spatiotemporal domain.[1−12] Unlike traditional vortex beams,[13−21] the phase vortices in STOVs evolve in both space and time, enabling new capabilities for integrated photonic chips and flat optics technology. However, conventional approaches relying on free-space optical components like spatial light modulators, lenses, and phased arrays[5,10] lack the integrability required for advanced photonic technologies. Recently, the emerging concept of "topological darkness" has shown promise for rapid phase manipulation in nanophotonics. Topological darkness refers to the presence, guaranteed by topological principles, of points where the intensity completely vanishes. These "dark" points are accompanied by optical phase singularities. They can be observed in complex light fields and can also be achieved in metasurfaces and other nanophotonic structures. The associated sharp phase changes near these singularities enable applications like ultrasensitive sensing.[22−25]

In this study, we demonstrate that photonic crystal (PhC) slabs possess abundant photonic bands and resonant modes, and as such, they exhibit lines of topological darkness in three-dimensional (3D) frequency−momentum space. By harnessing this resonance-enabled darkness of a PhC slab, we can imprint spatiotemporal optical vortices onto reflected light pulses, manifesting as inherent vortex lines within the pulse structure [Figure 1(a)].[26−30] We achieve this topological darkness via symmetry-protected complete conversion between circular polarizations. Using time-resolved spatial mapping at a fixed propagation distance, we provide the first observation of such vortex lines generated through the topological darkness in a PhC slab. PhC slabs, with their high design flexibility, allow for precise engineering of photonic dispersion, offering a pathway to customize the curvature of vortices and thus enabling advanced capabilities in pulse shaping. Our work positions photonic crystal slabs as versatile platforms for manipulating STOVs through topological darkness, opening new possibilities in spatiotemporal pulse shaping.

Let us start from the basic principle for imprinting a phase vortex into the optical pulse, harnessing the existence of topological darkness of a reflective two-dimensional (2D) photonic crystal (PhC) slab. The topological darkness here refers to singularities in co-polarized reflection for circular polarizations. The PhC slab structure we consider consists of a 2D periodic lattice pattern etched into a thin dielectric membrane with a mirror substrate underneath. This structure has reflection symmetry in the plane of the slab but no rotational symmetry within the 2D lattice plane [see Figure 1(a)]. Such a PhC slab supports guided resonances, which are modes confined by the periodic structure to propagate within the slab plane, yet

Received: November 10, 2023
Revised: January 8, 2024
Accepted: January 8, 2024

https://doi.org/10.1021/acs.nanolett.3c04348
Nano Lett. XXXX, XXX, XXX−XXX

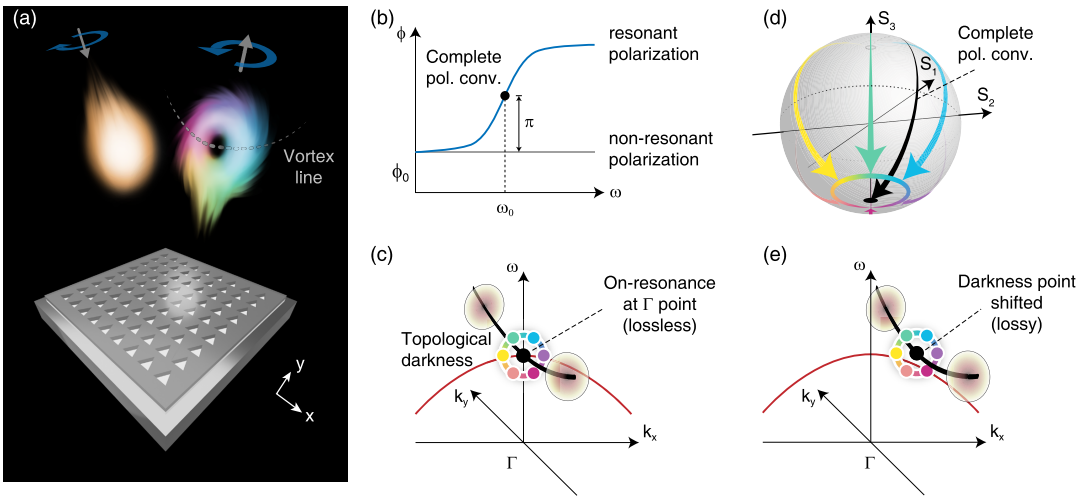

Figure 1. Basic principle of spatiotemporal optical vortex generation utilizing topological darkness of a photonic crystal slab. (a) Schematic of spatiotemporal optical vortex generation using topological darkness. A Gaussian pulse impinges on a reflective photonic crystal (PhC) slab structure consisting of a periodic pattern etched into a dielectric membrane positioned on a mirror substrate. The reflected pulse acquires a spatiotemporal optical vortex (STOV) structure containing an inherent curved vortex line (dashed gray curve). (b) When a guided resonance mode is excited by the incident light of the coupled polarization at normal incidence, the reflected light of that polarization acquires an extra phase that ranges continuously from 0 to 2π across the spectral range encompassing the resonance frequency ω_0. This phase modulation occurs only for the x/y linear polarization component in resonance with the external wave, enabling complete polarization conversion of circularly polarized light at ω_0. (c) Optical darkness and its associated topological phase vortex in the frequency−momentum (ω−$k_{\|}$) space. The complete polarization conversion point for circularly polarized light creates a singularity at ω_0, $k_{\|} = 0$, associated with the guided resonance dispersion (red curve). This singularity yields zero co-polarized reflectance (black dot) and exists robustly for nonzero k_y, forming a curved line of darkness (black curve). Slicing the ω−$k_{\|}$-space distribution of co-polarized reflectance by planes intersecting the line will give dark points in co-polarized reflectance. Incomplete polarization conversion occurs at points around the singularity, yielding nonzero co-polarized reflectance. The continuous color change of these points visualizes the phase vortex surrounding the dark point. (d) Complete polarization conversion at ω_0 follows a trajectory from one pole to the other on the Poincaré sphere (black arrowed curve). The surrounding trajectories correspond to incomplete conversion, and they yield elliptically polarized light, depicted by the colored curves between the poles. The ending points of these colored curves form a loop around the pole. (e) In the presence of material loss, the line of topological darkness displaces slightly from the $k_x = 0$ plane but remains intact in the ω−$k_{\|}$ space, as shown by the black curve.

they can also radiate out-of-plane.[31−33] These guided resonances have in-plane wavevectors $\mathbf{k}_{\|} = (k_x, k_y)$ that form photonic resonance bands inside the light cone.

With the help of guided resonances (whose frequencies and wavevectors forbid diffraction), complete polarization conversion can occur due to the selective coupling enforced by symmetry. We first consider the incident light in the plane defined by $\mathbf{k}_{\|} = (k_x, 0)$ and assume the materials composing the structure are lossless. Notably, the reflection symmetry of the PhC slab structure leads to an even/odd separation of the guided resonance modes at the Γ point [$\mathbf{k}_{\|} = (0, 0)$]. Under normal incidence, resonances with even symmetry, characterized by their even-symmetric electric field profile about the $x = 0$ reflection plane perpendicular to the slab, couple only to y-polarized light. Odd resonances, with an odd symmetry, couple to only x-polarized light. When one given guided resonance is excited by the normally incident light of the coupled polarization, it introduces an extra phase shift spanning 0 to 2π over the frequency domain to the reflected plane wave [Figure 1(b)], as derived from a temporal coupled mode theory[31−33] (see the Supporting Information for details):[34]

$$r_{\text{resonant}} = \frac{i(\omega_0 - \omega) - \gamma_0}{i(\omega_0 - \omega) + \gamma_0} \cdot r,\ r_{\text{non-resonant}} = r;$$

$$|r_{\text{resonant}}| = |r_{\text{non-resonant}}| = |r| = 1;$$

$$\arg(r_{\text{resonant}}/r_{\text{non-resonant}}) = \begin{cases} 0 (\omega \to -\infty) \\ \pi (\omega = \omega_0) \\ 2\pi (\omega \to +\infty) \end{cases} \quad (1)$$

Here, ω_0 and γ_0 are the resonance eigen-frequency and decay ratio (solely due to radiative damping), ω is the excitation frequency which is a real number, and r is the direct reflection coefficient if resonance is not excited. r_{resonant} and $r_{\text{non-resonant}}$ are the reflection coefficients through the resonant and non-resonant polarization channels, respectively, which are x or y polarizations depending on the symmetry of the resonance. At $\omega = \omega_0$, the extra π phase of r_{resonant} in the resonant scattering channel enables the PhC slab to function as a half-wave plate, which can completely convert the input circular polarization to the orthogonal circular polarization. This process corresponds to a trajectory from one pole (e.g., north pole) to the other (e.g., south pole) on the Poincaré sphere as shown by the black arrowed curve in Figure 1(d). In the vicinity of the complete conversion point where $\omega \neq \omega_0$ or $k_x \neq 0$, the conversion becomes incomplete, yielding elliptically polarized outgoing waves.

The resonant-induced polarization conversion for different (ω, k_x) values on a loop in the ω−k_x plane enclosing the complete-conversion point correspond to the colored curves

https://doi.org/10.1021/acs.nanolett.3c04348
Nano Lett. XXXX, XXX, XXX−XXX

shown in Figure 1(d), whose ending points also form a loop around the pole on the Poincaré sphere. Consequently, the complete conversion at $k_x = 0$, $\omega = \omega_0$ yields zero co-polarized reflectance in *either* left or right circular polarization, which is referred to as optical darkness [the black dot in Figure 1(b)]. This darkness point has a topological character; the incomplete conversion on the loop surrounding the dark point gives nonzero co-polarized reflectance and, crucially, winding phases that form a phase vortex in the $k_y = 0$ plane of the frequency−momentum (ω−$\mathbf{k}_{\parallel}$) space [Figure 1(c)].

We note that due to the topological nature the singularity persists for $k_y \neq 0$. Therefore, the topological dark points form a curved line in the 3D ω−$\mathbf{k}_{\parallel}$ space, as illustrated in Figure 1(c) by the black curve. The curvature and shape of this line of darkness, at which the co-polarized reflectance is zero, are associated with the photonic bands of guided resonance, but it does not reside on the bands exactly. With an oblique incidence ($k_y \neq 0$), not only the resonance but also the difference between direct reflection coefficients for x and y polarizations contribute to the circular polarization conversion. As a result, the required resonant phase $\arg(r_{\text{resonant}}/r_{\text{non-resonant}})$ deviates from π, making the complete conversion frequency displace from ω_0. Thus, in the lossless systems we discuss, the line of topological darkness touches the photonic band maximum or minimum at the Γ point ($\mathbf{k}_{\parallel} = 0$) but will shift away from the band dispersion for $k_x = 0$, $k_y \neq 0$. Notably, while the line of darkness shifts away from the guided resonance bands for oblique incidence, the structural mirror symmetry constrains the singularities to remain pinned to the $k_x = 0$ plane for both left and right circular polarizations in the lossless case under discussion, as shown in Figure 1(c). If the mirror symmetry is broken, the lines of topological darkness persist, although they are no longer anchored to the mirror plane. Examples of simulated scenarios where mirror symmetry is broken can be found in the Supporting Information.[34]

Upon illumination of the PhC slab with an input pulse that spans the spectral-wavevector range of the line of topological darkness in the ω−$\mathbf{k}_{\parallel}$ space, a vortex line in real space is formed in the reflected pulse profile. This vortex line is an inherent structure of the pulse, observable in a single snapshot of the spatial pulse profile at a fixed time or in the space−time profile at a fixed propagation distance. It represents the manifestation of the line of topological darkness in the reciprocal spaces of frequency and wavevector, i.e., time and space. As the pulse propagates, the vortex line, anchored by the topological darkness in frequency−momentum space, moves with the pulse, highlighting its inherent structure within the pulse.

In practice, material loss cannot be eliminated, especially in the optical range. In the presence of material loss, the Γ-point resonance can no longer convert the circular polarization completely, because the loss will reduce the reflectance for the coupled polarization. However, since the optical darkness is topologically robust, the line of darkness displaces slightly from $k_x = 0$ but remains intact in the ω−$\mathbf{k}_{\parallel}$ space [Figure 1(e)]. Constrained by the mirror symmetry, the lines of darkness for left and right circularly co-polarized reflection will be mirror-symmetric about the $k_x = 0$ plane. Please see the Supporting Information[34] for simulated examples demonstrating the impact of material loss.

To experimentally observe these photonic crystal-slab-enabled STOVs, we designed and fabricated a PhC structure with the required symmetry and subsequently measured its optical response.

The structure used in our experiments is illustrated in Figure 2(a). It consists of a square lattice pattern of triangular holes

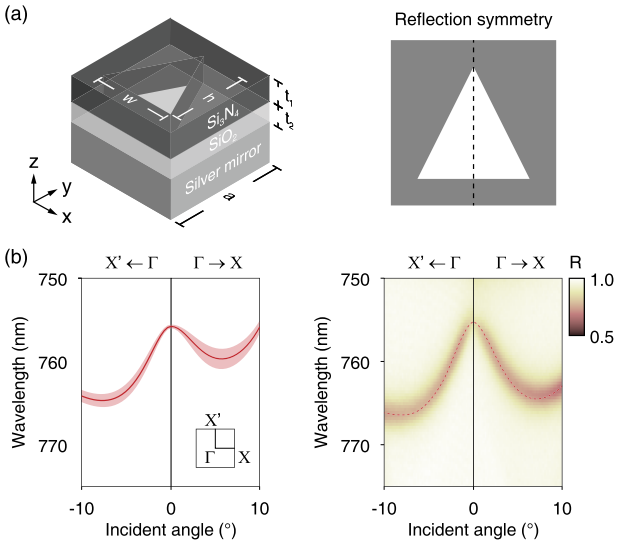

Figure 2. Photonic crystal slab sample design and characteristics. (a) The photonic crystal slab structure consists of a square lattice of triangular holes etched into a silicon nitride (Si_3N_4) membrane positioned on top of a silver mirror substrate. Key dimensions are labeled, including the lattice constant a, hole width/height w/h, and Si_3N_4 and silica layer thicknesses t_1 and t_2. The structure has reflection symmetry with respect to the Γ−X′ direction. (b) Left: The guided resonance band used to generate the spatiotemporal optical vortex. The solid line and the shaded area plot the real part ω_0 and the imaginary part γ_0 (decay ratio) of the resonance's eigen-frequency, respectively. Right: Measured unpolarized reflectance spectra show dips at the guided resonance frequencies. The resonance wavelengths match well between the simulated band structure and the measured reflectance. The Γ point corresponds to a normal incidence.

etched into a silicon nitride (Si_3N_4) membrane with a silver mirror substrate underneath. The lattice constant is $a = 560$ nm, the hole width and height are $w = h = 400$ nm, and the Si_3N_4 membrane thickness is $t_1 = 140$ nm above a $t_2 = 100$ nm silica (SiO_2) spacer layer. This structure has reflection symmetry in the slab plane about the Γ−X′ direction ($x = 0$).

The left panel of Figure 2(b) shows the dispersion of the guided resonance band that we used to generate the STOV. The dispersion of this resonance band shows good agreement with the measured *unpolarized* reflectance spectra in the right panel of Figure 2(b). Here, the Γ point corresponds to the normal incidence. In the left panel, the red curve shows the simulated dispersion of the guided resonance, while the shaded area indicates the bandwidth (twice the decay ratio γ_0). The right panel shows the dips in the experimentally measured unpolarized reflectance. Guided resonances cause absorption of the unpolarized incident wave, leading to dips in reflectance, and hence, the unpolarized reflectance dips can be used to indicate the guided resonance.

Our experimental measurements confirm the predicted existence of topological darkness in the 3D frequency−momentum space, as shown in Figure 3. Figure 3(a) displays the angle-dependent co-circularly polarized (left circular polarization) reflectance maps sliced at different wavelengths. These maps reveal zero reflectance points, which represent the intersections of the iso-frequency planes and the line of topological darkness in the frequency−momentum space. At

https://doi.org/10.1021/acs.nanolett.3c04348
Nano Lett. XXXX, XXX, XXX−XXX

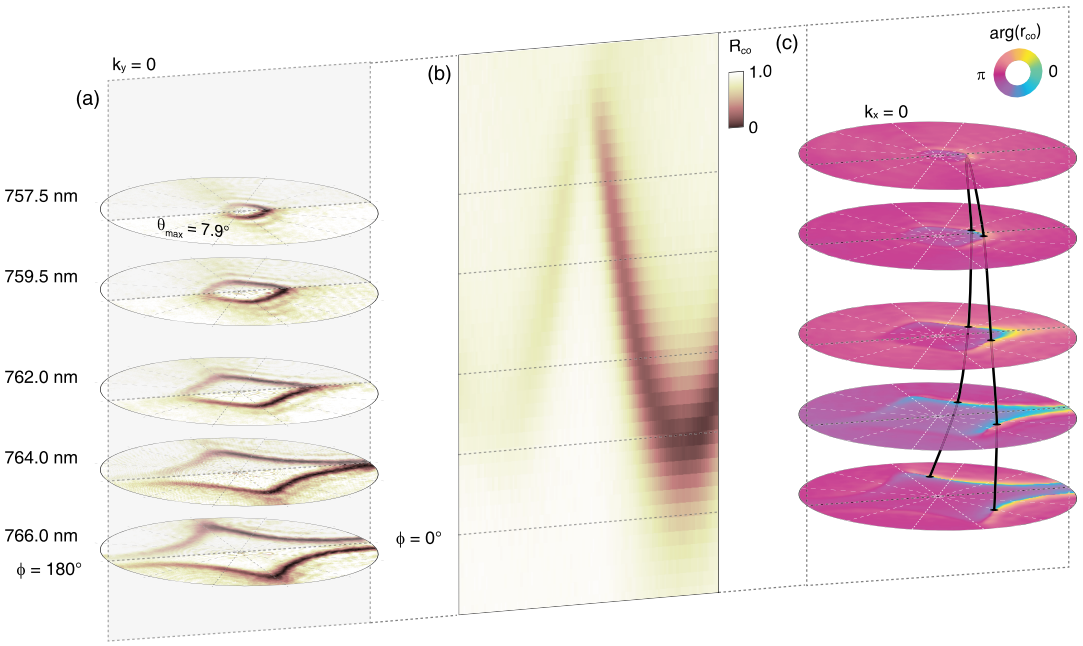

Figure 3. Experimental confirmation of the frequency−momentum space topological darkness. (a) When co-polarized reflectance maps are measured at various wavelengths, they exhibit zero co-polarized reflectance points embedded in arcs of dark regions corresponding to intersections with the line of topological darkness, as we schematically illustrated in Figure 1(a). The dark regions merge at around 758−759 nm, marking the turning point of the curved line of darkness which displaces from the $k_x = 0$ plane and the resonance dispersion due to loss. (b) The vertical slice of co-polarized reflectance at $k_y = 0$ shows a dark region with the embedded zero point representing the intersection with the curved line of darkness. The vertical slicing plane $k_y = 0$ is marked by a shadowed plane in Figure 3(a). The frequencies measured in Figure 3(a) are marked by dashed lines here. (c) Reflective phase maps visualize the curved singular line of darkness (black curve). Two phase vortices with opposite topological charge (±1) appear in lower plots at longer wavelengths and annihilate as they converge around 758 nm.

wavelengths longer than 757.5 nm, the maps exhibit arcs of dark regions, each containing embedded zero reflectance points. Around 758−759 nm, these separate dark arcs merge into one, marking the turning point of the line of darkness. This merging shows a displacement from the $k_x = 0$ plane, attributed to material loss. On the other hand, Figure 3(b) shows a vertical momentum-wavelength slice of the co-polarized reflectance at $k_y = 0$, and the point of zero co-polarized reflectance is embedded in the dark region. The reflective phase plots sliced at different wavelengths in Figure 3(c) directly visualize the curved line of darkness (marked by the black curve). There are two phase vortices of opposite charge (±1) at longer wavelengths in the lower plots, which annihilate as they converge and merge at around 758 nm. These observations from Figure 3 validate the existence of a line of topological darkness in the 3D frequency−momentum space, confirming the PhC slab's ability to produce such a feature via complete polarization conversion. Simulated 3D maps of co-polarized reflectance and reflective phase corresponding to the experimentally measured Figure 3 are available in the Supporting Information.[34]

In order to directly observe the spatiotemporal vortex line imprinted by the PhC slab, we performed time-resolved measurements of the reflected pulse. A femtosecond laser pulse impinges the sample at normal incidence, and the reflected pulse passes through a convex lens before being measured by a space−time-resolved imaging system (see the Supporting Information for details).[34] By fixing the imaging plane at a particular propagation distance z from the sample, we map the x−y spatial distribution of the pulse at different time instances t. As a result, a 3D x−y−t space−time map of the pulse profile at fixed z can be constructed, revealing the structure of the vortex line singularity. At each time instance, the x−y map shows the intersection of the vortex line with the fixed z plane, manifesting as zero intensity points. As time progresses, the pulse containing the vortex line transverse to the propagation direction will pass through the chosen z plane. As a result, the spatial movement of the zero points at different t traces the spatiotemporal vortex line singularity in the fixed z plane.

Figure 4(b) shows space−time maps of the reflected co-polarized pulse sliced at different fixed y-positions. At each y-position, we map out the intensity of the pulse as a function of the x-position and time t. As shown in the space−time maps in Figure 4(b), a zero point appears in each y-cut, corresponding to the intersection of the constant-y plane with the vortex line singularity. As evidenced by the space−time maps in Figure 4(b), the non-monotonous variation in the x−t position of zero points with y underscores the complex, curved nature of the vortex line in space and time.

Complementary to the y-cuts, Figure 4(c) displays the interference patterns of the reflected pulse at different fixed t-delays in the fixed z plane. The fork-like fringe dislocations in these interference patterns signify phase singularities arising from intersections of the t-slices and the vortex line. Notably, the pair of phase singularities observed on each t-slice have opposite topological charges (shown by the opposite directions of the folk-like fringes), arising from the same curved vortex line intersecting the constant-t plane at two points.

By extracting the positions of singularities at each t-delay, we can plot the curved vortex line explicitly in space−time with z fixed, as shown by the dashed gray curve in Figure 4(a). This curve exhibits a clear curvature in the space−time domain. Clearly, our time-resolved measurements in Figure 4 directly map out the spatiotemporal vortex imprinted on the reflected pulse by the PhC slab. The observed curved vortex line

https://doi.org/10.1021/acs.nanolett.3c04348
Nano Lett. XXXX, XXX, XXX−XXX

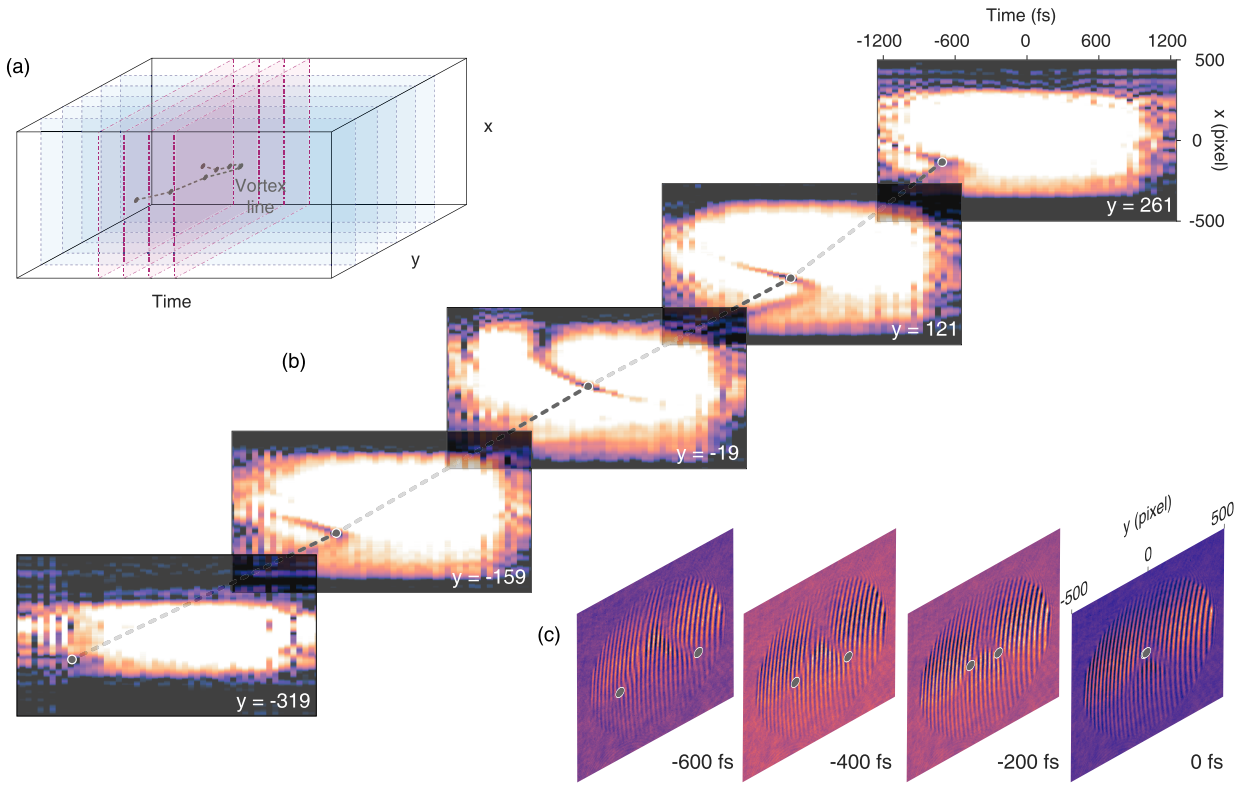

Figure 4. Direct mapping of the imprinted spatiotemporal vortex through time-resolved measurements. (a) Schematic showing the spatial regions where *y*-cuts (blue dashed planes) and *t*-cuts (red dashed planes) are taken to map out the vortex line in space−time. The extracted trajectory of the vortex line singularity is marked by a dashed gray curve. (b) Measured space−time intensity maps of the reflected pulse at five different fixed *y*-positions. At each *y*-position, the pulse's intensity is mapped as a function of *x*-position and time delay *t*. Zero singularities are observed, corresponding to intersections between the constant-*y* plane and the vortex line. (c) *x*−*y* interference patterns of the reflected pulse at four different time delays *t*. Fork-like fringe dislocations reveal phase singularities in the *t*-slices. The observed pairs of dislocations exhibit opposite topological charges, consistent with the fact that each *t*-slice cuts the curved vortex line at two points.

trajectory and phase singularities confirm the vortex topology enabled by the complete polarization conversion.

In summary, we have demonstrated the generation of spatiotemporal optical vortices by leveraging the topological darkness of a PhC slab. Through the guided resonances in a mirror-based 2D photonic crystal slab, we imprint vortex singularities onto an ultrashort reflected pulse via complete polarization conversion enforced by symmetry. This process generates a vortex line, a defining feature of these spatiotemporal optical vortices. By doing so, we overcome some limitations of conventional free-space optical components, exhibiting the potential of resonance-enabled topological darkness.

Both frequency−momentum space maps and direct time-resolved measurements confirm the emergence of the vortex line, which aligns with our predictions. Notably, our work marks the first observation and three-dimensional spatiotemporal mapping of spatiotemporal optical vortices generated through topological darkness in a photonic crystal slab, establishing the versatility of these slabs in generating STOVs.

Looking forward, the dispersion of the photonic crystal slab can be engineered to modify the curvature of the vortex line (see simulated examples in the Supporting Information[34]), providing a promising avenue for advanced spatiotemporal beam shaping. This suggests significant potential for the vortex line in the development of next-generation optical systems.

■ ASSOCIATED CONTENT

Supporting Information

The Supporting Information is available free of charge at https://pubs.acs.org/doi/10.1021/acs.nanolett.3c04348.

Theoretical analysis, numerical and simulated examples, and experimental details for the photonic crystal slab spatiotemporal vortex generation are provided. A temporal coupled mode theory proves the existence of complete circular polarization conversion singularities (topological darkness) in the photonic crystal slab system, forming phase vortex lines in momentum space. Simulated examples show the impact of material loss, symmetry breaking, and structure tuning on the topological darkness. The experimental setup splits femtosecond laser pulses into sample and reference arms. The sample pulse is focused on the photonic crystal slab sample, and its reflection interferes with the tilted reference pulse. Their interference pattern, recorded on a camera, contains signatures of the spatiotemporal optical vortices generated by the photonic crystal slab. (PDF)

■ AUTHOR INFORMATION

Corresponding Authors

Wenzhe Liu − *Department of Physics, The Hong Kong University of Science and Technology, Hong Kong 999077, China;* orcid.org/0000-0002-6582-4161; Email: wliubh@connect.ust.hk

https://doi.org/10.1021/acs.nanolett.3c04348
Nano Lett. XXXX, XXX, XXX−XXX

Lei Shi − *State Key Laboratory of Surface Physics, Key Laboratory of Micro- and Nano-Photonic Structures (Ministry of Education), and Department of Physics, Fudan University, Shanghai 200433, China; Institute for Nanoelectronic Devices and Quantum Computing, Fudan University, Shanghai 200438, China; Collaborative Innovation Center of Advanced Microstructures, Nanjing University, Nanjing 210093, China*; Email: lshi@fudan.edu.cn

Jian Zi − *State Key Laboratory of Surface Physics, Key Laboratory of Micro- and Nano-Photonic Structures (Ministry of Education), and Department of Physics, Fudan University, Shanghai 200433, China; Institute for Nanoelectronic Devices and Quantum Computing, Fudan University, Shanghai 200438, China; Collaborative Innovation Center of Advanced Microstructures, Nanjing University, Nanjing 210093, China*; Email: jzi@fudan.edu.cn

C. T. Chan − *Department of Physics, The Hong Kong University of Science and Technology, Hong Kong 999077, China*; orcid.org/0000-0002-9335-8110; Email: phchan@ust.hk

Authors

Jiajun Wang − *State Key Laboratory of Surface Physics, Key Laboratory of Micro- and Nano-Photonic Structures (Ministry of Education), and Department of Physics, Fudan University, Shanghai 200433, China*

Yang Tang − *State Key Laboratory of Surface Physics, Key Laboratory of Micro- and Nano-Photonic Structures (Ministry of Education), and Department of Physics, Fudan University, Shanghai 200433, China*

Xinhao Wang − *State Key Laboratory of Surface Physics, Key Laboratory of Micro- and Nano-Photonic Structures (Ministry of Education), and Department of Physics, Fudan University, Shanghai 200433, China*

Xingqi Zhao − *State Key Laboratory of Surface Physics, Key Laboratory of Micro- and Nano-Photonic Structures (Ministry of Education), and Department of Physics, Fudan University, Shanghai 200433, China*

Complete contact information is available at: https://pubs.acs.org/10.1021/acs.nanolett.3c04348

Author Contributions

[⊥]W.L., J.W., Y.T.: Contributed equally to this work.

Notes

The authors declare no competing financial interest.

■ ACKNOWLEDGMENTS

This work is supported by National Natural Science Foundation of China (No. 12234007, No. 12221004, and No. 12321161645), National Key Research and Development Program of China (2023YFA1406900, 2022YFA1404800, and 2021YFA1400603), Major Program of National Natural Science Foundation of China (T2394481), and Science and Technology Commission of Shanghai Municipality (23DZ2260100, 22142200400, 21DZ1101500, and 2019SHZDZX01). Work done in Hong Kong is supported by Research Grants Council (RGC) of Hong Kong (AoE/P-502/20, CRS_HKUST601/23, 16310422). J.W. is further supported by China National Postdoctoral Program for Innovative Talents (BX20230079) and China Postdoctoral Science Foundation (2023M740721).

■ REFERENCES

(1) Dror, N.; Malomed, B. A. Symmetric and asymmetric solitons and vortices in linearly coupled two-dimensional waveguides with the cubic-quintic nonlinearity. *Physica D* **2011**, *240*, 526−541.

(2) Bliokh, K. Y.; Nori, F. Spatiotemporal vortex beams and angular momentum. *Phys. Rev. A* **2012**, *86*, No. 033824.

(3) Jhajj, N.; Larkin, I.; Rosenthal, E. W.; Zahedpour, S.; Wahlstrand, J. K.; Milchberg, H. M. Spatiotemporal Optical Vortices. *Phys. Rev. X* **2016**, *6*, No. 031037.

(4) Hancock, S. W.; Zahedpour, S.; Goffin, A.; Milchberg, H. M. Free-space propagation of spatiotemporal optical vortices. *Optica* **2019**, *6*, 1547.

(5) Chong, A.; Wan, C.; Chen, J.; Zhan, Q. Generation of spatiotemporal optical vortices with controllable transverse orbital angular momentum. *Nat. Photonics* **2020**, *14*, 350−354.

(6) Bliokh, K. Y. Spatiotemporal Vortex Pulses: Angular Momenta and Spin-Orbit Interaction. *Phys. Rev. Lett.* **2021**, *126*, No. 243601.

(7) Hancock, S. W.; Zahedpour, S.; Milchberg, H. M. Mode Structure and Orbital Angular Momentum of Spatiotemporal Optical Vortex Pulses. *Phys. Rev. Lett.* **2021**, *127*, No. 193901.

(8) Cao, Q.; Chen, J.; Lu, K.; Wan, C.; Chong, A.; Zhan, Q. Non-spreading Bessel spatiotemporal optical vortices. *Science Bulletin* **2022**, *67*, 133−140.

(9) Bliokh, K. Y. Orbital angular momentum of optical, acoustic, and quantum-mechanical spatiotemporal vortex pulses. *Phys. Rev. A* **2023**, *107*, L031501.

(10) Ge, H.; Liu, S.; Xu, X.-Y.; Long, Z.-W.; Tian, Y.; Liu, X.-P.; Lu, M.-H.; Chen, Y.-F. Spatiotemporal Acoustic Vortex Beams with Transverse Orbital Angular Momentum. *Phys. Rev. Lett.* **2023**, *131*, No. 014001.

(11) Porras, M. A. Transverse Orbital Angular Momentum of Spatiotemporal Optical Vortices. *Progress In Electromagnetics Research* **2023**, *177*, 95−105.

(12) Smirnova, D. A.; Nori, F.; Bliokh, K. Y. Water-Wave Vortices and Skyrmions. 2023, arXiv 2308.03520. https://arxiv.org/abs/2308.03520 (accessed January 7, 2024).

(13) Allen, L.; Beijersbergen, M. W.; Spreeuw, R. J. C.; Woerdman, J. P. Orbital angular momentum of light and the transformation of Laguerre-Gaussian laser modes. *Phys. Rev. A* **1992**, *45*, 8185−8189.

(14) Bliokh, K. Y. Geometrical Optics of Beams with Vortices: Berry Phase and Orbital Angular Momentum Hall Effect. *Phys. Rev. Lett.* **2006**, *97*, No. 043901.

(15) Dennis, M. R.; O'Holleran, K.; Padgett, M. J. *Progress in Optics*; Elsevier: 2009; Vol. *53*, pp 293−363.

(16) Chen, S.; Cai, Y.; Li, G.; Zhang, S.; Cheah, K. W. Geometric metasurface fork gratings for vortex-beam generation and manipulation. *Laser & Photonics Reviews* **2016**, *10*, 322−326.

(17) Huang, C.; Zhang, C.; Xiao, S.; Wang, Y.; Fan, Y.; Liu, Y.; Zhang, N.; Qu, G.; Ji, H.; Han, J.; Ge, L.; Kivshar, Y.; Song, Q. Ultrafast control of vortex microlasers. *Science* **2020**, *367*, 1018−1021.

(18) Yang, Y.; Qiu, C.-W. *Electromagnetic Vortices*; John Wiley & Sons, Ltd: 2021; Chapter 7, pp 223−244.

(19) Ni, J.; Huang, C.; Zhou, L.-M.; Gu, M.; Song, Q.; Kivshar, Y.; Qiu, C.-W. Multidimensional phase singularities in nanophotonics. *Science* **2021**, *374*, No. eabj0039.

(20) Zhang, X.; Huang, L.; Zhao, R.; Wei, Q.; Li, X.; Geng, G.; Li, J.; Li, X.; Wang, Y.; Zhang, S. Multiplexed Generation of Generalized Vortex Beams with On-Demand Intensity Profiles Based on Metasurfaces. *Laser & Photonics Reviews* **2022**, *16*, No. 2100451.

(21) Wang, H.; Wang, H.; Ruan, Q.; Chan, J. Y. E.; Zhang, W.; Liu, H.; Rezaei, S. D.; Trisno, J.; Qiu, C.-W.; Gu, M.; Yang, J. K. W. Coloured vortex beams with incoherent white light illumination. *Nat. Nanotechnol.* **2023**, *18*, 264−272.

(22) Kravets, V. G.; Schedin, F.; Jalil, R.; Britnell, L.; Gorbachev, R. V.; Ansell, D.; Thackray, B.; Novoselov, K. S.; Geim, A. K.; Kabashin, A. V.; Grigorenko, A. N. Singular phase nano-optics in plasmonic metamaterials for label-free single-molecule detection. *Nat. Mater.* **2013**, *12*, 304−309.

(23) Malassis, L.; Massé, P.; Tréguer-Delapierre, M.; Mornet, S.; Weisbecker, P.; Barois, P.; Simovski, C. R.; Kravets, V. G.; Grigorenko, A. N. Topological Darkness in Self-Assembled Plasmonic Metamaterials. *Adv. Mater.* **2014**, *26*, 324−330.
(24) Ermolaev, G.; et al. Topological phase singularities in atomically thin high-refractive-index materials. *Nat. Commun.* **2022**, *13*, 2049.
(25) Tselikov, G. I.; Danilov, A.; Shipunova, V. O.; Deyev, S. M.; Kabashin, A. V.; Grigorenko, A. N. Topological Darkness: How to Design a Metamaterial for Optical Biosensing with Ultrahigh Sensitivity. *ACS Nano* **2023**, *17*, 19338−19348.
(26) Wang, H.; Guo, C.; Jin, W.; Song, A. Y.; Fan, S. Engineering arbitrarily oriented spatiotemporal optical vortices using transmission nodal lines. *Optica* **2021**, *8*, 966.
(27) Doskolovich, L. L.; Kashapov, A. I.; Bezus, E. A.; Bykov, D. A. Spatiotemporal optical differentiation and vortex generation with metal-dielectric-metal multilayers. *Phys. Rev. A* **2022**, *106*, No. 033523.
(28) Kashapov, A. I.; Bezus, E. A.; Bykov, D. A.; Doskolovich, L. L. Plasmonic Generation of Spatiotemporal Optical Vortices. *Photonics* **2023**, *10*, 109.
(29) Zhou, Y.; Zhan, J.; Xu, Z.; Shao, Y.; Wang, Y.; Dang, Y.; Zhang, S.; Yungui, M. Electromagnetic Spatiotemporal Differentiators. 2023, arXiv 2308.03797. https://arxiv.org/abs/2308.03797 (accessed January 7, 2024).
(30) Zhang, H.; Sun, Y.; Huang, J.; Wu, B.; Yang, Z.; Bliokh, K. Y.; Ruan, Z. Topologically crafted spatiotemporal vortices in acoustics. *Nat. Commun.* **2023**, *14*, 6238.
(31) Johnson, S. G.; Fan, S.; Villeneuve, P. R.; Joannopoulos, J. D.; Kolodziejski, L. A. Guided modes in photonic crystal slabs. *Phys. Rev. B* **1999**, *60*, 5751−5758.
(32) Fan, S.; Joannopoulos, J. Analysis of guided resonances in photonic crystal slabs. *Phys. Rev. B* **2002**, *65*, No. 235112.
(33) Fan, S.; Suh, W.; Joannopoulos, J. D. Temporal coupled-mode theory for the Fano resonance in optical resonators. *J. Opt. Soc. Am. A* **2003**, *20*, 569.
(34) See the Supporting Information.

https://doi.org/10.1021/acs.nanolett.3c04348
Nano Lett. XXXX, XXX, XXX−XXX